

Vortex and dipole solitons in complex two-dimensional nonlinear lattices

Mark J. Ablowitz

Department of Applied Mathematics, University of Colorado, Boulder, Colorado 80309-0526, USA

Nalan Antar and İlkey Bakırtaş*

Department of Mathematics, Istanbul Technical University, Maslak 34469, Istanbul, Turkey

Boaz Ilan

School of Natural Sciences, University of California, Merced, California 95344, USA

(Received 28 July 2011; revised manuscript received 7 August 2012; published 4 September 2012)

Using computational methods, it is found that the two-dimensional nonlinear Schrödinger (NLS) equation with a quasicrystal lattice potential admits multiple dipole and vortex solitons. The linear and the nonlinear stability of these solitons is investigated using direct simulations of the NLS equation and its linearized equation. It is shown that certain multiple vortex structures on quasicrystal lattices can be linearly unstable but nonlinearly stable. These results have application to investigations of localized structures in nonlinear optics and Bose-Einstein condensates.

DOI: [10.1103/PhysRevA.86.033804](https://doi.org/10.1103/PhysRevA.86.033804)

PACS number(s): 42.65.Tg, 42.65.Jx

I. INTRODUCTION

Dipole and higher-phase vortex solitons and other nonlinearly localized structures with a complex phase have attracted considerable interest in recent years. Vortex-type solitons in the presence of an (optically or magnetically) induced lattice have been investigated analytically and experimentally in Bose-Einstein condensates (BECs) [1,2] and in optical Kerr media [3–8].

Such structures appear as special solutions of the focusing two-dimensional cubic nonlinear Schrödinger (NLS) equation with an external potential. The stability of these solitons is important to applications. Rigorous stability theory of *fundamental* (positive) solitons is well established [9–12]. In nonhomogeneous media it has been shown that solitons can undergo self-focusing and drift (tunneling) instabilities [13–16]. Unfortunately, the analytic stability theory of solitons possessing a *complex phase structure* and on *quasicrystal lattices* is not sufficiently well developed. Nevertheless this issue can be studied computationally. Earlier computational studies have shown that vortex-type solitons on a periodic lattice can be stable within certain ranges of parameters [17–19] and also in saturable (e.g., photorefractive) media [20–22].

Thus far, there have been very few studies of complex-phase solutions in the presence of quasicrystal and other complex potentials [23], while the majority of studies consider crystal-type (periodic) potentials. As a result of this fact, both the numerical existence and the (computational) stability properties of multiple vortex solitons on background quasicrystal lattices have remained relatively unexplored.

In this study, we compute soliton solutions of the focusing cubic (2 + 1)-dimensional NLS equation with quasicrystal (e.g., Penrose) potentials and study their stability. The gov-

erning equation is

$$iu_z + \Delta u + |u|^2 u - V(x, y)u = 0, \quad (1)$$

where z plays the role of time (or distance) and $V(x, y)$ models the induced potential. We explore both linear and nonlinear stability numerically. In optics, $u(x, y, z)$ corresponds to the complex-valued, slowly varying amplitude of the electric field in the xy plane propagating in the z direction, $\Delta u \equiv u_{xx} + u_{yy}$ corresponds to diffraction, the cubic term in u originates from the nonlinear (Kerr) change of the refractive index, and $V(x, y)$ is an external optical potential that can be written as the intensity of a sum of N phase-modulated plane waves, i.e. (see [19]),

$$V(x, y) = \frac{V_0}{N^2} \left| \sum_{n=0}^{N-1} e^{i\vec{k}_n \cdot \vec{x}} \right|^2, \quad (2)$$

where $V_0 > 0$ is constant and corresponds to the peak depth of the potential, i.e., $V_0 = \max_{x, y} V(x, y)$, $\vec{x} = (x, y)$, and \vec{k}_n is a wave vector defined by $(k_x^n, k_y^n) = [K \cos(2\pi n/N), K \sin(2\pi n/N)]$. The potential given in (2) with $N = 2, 3, 4, 6$ yields periodic lattices. All other values of N correspond to quasicrystals, which have a local symmetry around the origin and long-range order, but, unlike periodic crystals, are not invariant under spatial translations.

In this work, as the external potential, we consider the quasicrystal lattice corresponding to $N = 5$ in Eq. (2). In particular, the quasicrystal with $N = 5$ is often called the Penrose tiling [24]. Contour images of two potentials corresponding to periodic ($N = 4$) and Penrose quasicrystals ($N = 5$) are displayed all with $V_0 = 10$ and $K = 1$ in Fig. 1. Freedman *et al.* observed solitons in Penrose and other quasicrystal lattices generated by the optical induction method [6].

Using the method of spectral renormalization, we numerically find both multiple vortex and dipole solitons on quasicrystal “Penrose” ($N = 5$) background lattices. The linear and nonlinear (in)stabilities are also examined for these localized structures by direct computations of Eq. (1) and

*Corresponding author: ilkayb@itu.edu.tr

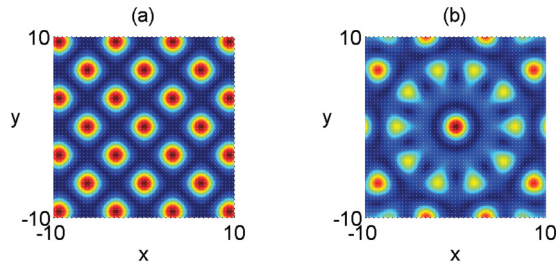


FIG. 1. (Color online) Contour images of lattices: (a) periodic ($N = 4$); (b) Penrose ($N = 5$). Both with $V_0 = 10$ and $K = 1$.

its linearized equation. The initial conditions are taken to be a vortex or dipole with 1% random complex noise. An interesting result of the stability analysis is that the vortex (dipole) solitons can be nonlinearly stable while being linearly unstable (see Figs. 15 and 23).

II. SPECTRAL RENORMALIZATION

In order to compute localized solutions (i.e., soliton solutions) to nonlinear evolution equations, various techniques have been used. For detailed information on numerical methods for solving wave equations, see [25]. Below we mention some of these methods. Shooting, relaxation techniques, and the self-consistency method have been around for decades, but they are not always efficient and/or applicable for multi-dimensional problems. A different method was introduced by Petviashvili [26] to construct localized solutions in the two-dimensional Korteweg–de Vries equation (usually referred to as the Kadomtsev–Petviashvili equation). The idea behind Petviashvili’s method is to transform the underlying governing equation to Fourier space and determine a convergence factor based upon the degree (homogeneity) of a single nonlinear term. This method has been extensively used to find localized solutions in a wide range of nonlinear systems. It can be successfully applied to nonlinear systems only if the degree of the nonlinearity is fixed in the associated evolution equation. In fact, in nonlinear optics, many equations involve nonlinearities with different homogeneities, such as cubic–quintic, or even lack of homogeneity, as in saturable nonlinearity.

Ablowitz and Musslimani [27] proposed a generalized numerical scheme for computing solitons in nonlinear wave guides called spectral renormalization. The essence of the method is to transform the governing equation into Fourier space and find a nonlinear nonlocal integral equation coupled to an algebraic equation. The coupling prevents the numerical scheme from diverging. The optical mode is then obtained from an iteration scheme, which converges rapidly. This method can efficiently be applied to a large class of problems including higher-order nonlinear terms with different homogeneities.

In recent years, Lakoba and Yang in [28] proposed generalizations of Petviashvili’s iteration method to scalar and vector Hamiltonian equations with arbitrary forms of nonlinearity and potential functions. Later they extended this method to eliminate from the iterations a mode that is responsible for either the divergence or the slow convergence of the iterations [29]. The conjugate gradient method is yet another iterative method for solving linear systems. Lately, the

conjugate gradient method was modified for finding solitary waves of nonlinear evolution equations [30,31].

In this work, we use the spectral renormalization method. To do this, we seek a soliton solution of Eq. (1) in the form $u(x, y, z) = f(x, y)e^{-i\mu z}$ where $f(x, y)$ is a complex-valued function and μ is the propagation constant (frequency). Substituting this form of solution into Eq. (1), the following nonlinear equation for f is obtained:

$$\Delta f + [\mu + |f|^2 - V(x, y)]f = 0. \quad (3)$$

After applying the Fourier transformation to Eq. (3), in order to avoid a possible singularity, we add a term $r\hat{f}$ on both sides of Eq. (3), where $r > 0$ is typically chosen as $r = 20$ or larger, up to $r = 100$, in order to obtain convergence, depending on the numerical values of the eigenvalue μ or the lattice depth V_0 . This procedure leads us to the following equation:

$$\hat{f}(v) = \hat{R}[\hat{f}] \equiv \frac{(r + \mu)\hat{f} + \mathcal{F}\{|f|^2 - V(x, y)\}f}{r + |v|^2}. \quad (4)$$

Here \mathcal{F} denotes the Fourier transform, and $v = (v_x, v_y)$ are Fourier variables. We introduce a new field variable $f(x, y) = \lambda w(x, y)$, where $\lambda \neq 0$ is a constant to be determined at every step. The iteration method takes the form $\hat{w}_{m+1} = \lambda_m^{-1} \hat{R}[\lambda_m \hat{w}_m]$, $m = 0, 1, 2, \dots$, where λ_m satisfies the associated algebraic condition

$$\iint_{-\infty}^{\infty} |\hat{w}_m(v)|^2 dv = \lambda_m^{-1} \iint_{-\infty}^{\infty} \hat{R}[\lambda_m \hat{w}_m] \hat{w}_m^*(v) dv. \quad (5)$$

Thus, the soliton is obtained from a convergent iterative scheme. The initial starting point $w_0(x, y)$ is typically chosen to be localized; e.g., a Gaussian. In this work, in order to investigate the dipole and vortex structures, as initial condition, we use multihumped Gaussians (two-humped for dipoles, five-humped and ten-humped for vortex modes) centered at either maxima or minima on the lattice structure. The iteration continues until $|w_{n+1} - w_n| < 10^{-8}$ and $\delta = |\lambda_{m+1}/\lambda_m - 1|$ reaches 10^{-8} . Convergence is obtained quickly when the mode is strongly localized in the band gap. This occurs when the linearized spectrum is in the semi-infinite band gap. Further, it is observed that the mode becomes more extended as μ gets closer to the band gap edge, and convergence of such a mode slows down significantly during the iteration process.

III. NUMERICAL INVESTIGATION OF VORTEX AND DIPOLE SOLITONS

In this section, we show the existence of both vortex and dipole solitons centered at the lattice minima and maxima for a Penrose potential. Hereafter, the potential depth is set to $V_0 = 10$.

For the spectral renormalization, we used the following initial conditions, centered at the lattice minima and maxima:

$$w_0(x, y, 0) = A \sum_{n=0}^{M-1} e^{-[(x+x_n)^2 + (y+y_n)^2] + i\theta_n}, \quad (6)$$

where x_n and y_n represent the location of vortex solitons, θ_n is the phase difference, M corresponds to the number of humps, and A is a positive integer.

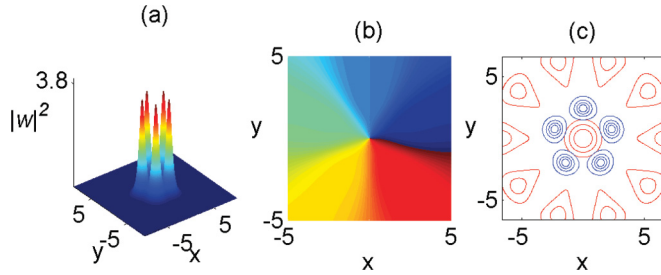


FIG. 2. (Color online) (a) Vortex profile with five humps centered at the lattice minimum close to the lattice center, with $r = 2.3918$; (b) the phase structure of the vortex; (c) the contour plot of the vortex humps superimposed on the underlying Penrose potential ($N = 5$).

A. Vortex solitons on the lattice minima

Vortex solitons for the Penrose quasicrystal potential are found numerically with the initial condition defined in Eq. (6). Here, $x_n, y_n,$ and θ_n are given as

$$x_n = r \cos \theta_n, \quad y_n = r \sin \theta_n, \quad \theta_n = \frac{m\pi n}{N} - \frac{\pi}{2N}. \quad (7)$$

In order to generate a five-hump vortex at the minimum of the lattice, we used Eqs. (2) and (7) with $m = 2$ and $M = 5$. Here, we investigated two different cases; later we show that they have different stability properties. In both cases, the propagation constant is taken to be $\mu = -2$.

In the first case, the vortex humps are chosen to be located close to the center of the lattice. In order to generate this vortex, we took $A = 3$ and $r = 2.3918$ (numerical convergence of the mode can be quite sensitive to the value of r). The vortex profiles, the phase structures, and the contour plots superimposed on the underlying Penrose potential are shown in Fig. 2.

Vortex humps further away from the center of the lattice (the global maximum of the lattice) were obtained by changing the previous location of the initial condition by taking $r = 5.3918$. The vortex profile, phase structure, and contour plots superimposed on the underlying Penrose potential of vortex solitons at a lattice minimum away from the lattice center are shown in Fig. 3.

A ten-hump vortex at a lattice minimum is also obtained; here we took $m = 1, M = 10, A = 1,$ and $r = 5.2553$. The propagation constant is taken to be $\mu = -2$. The vortex profile, the phase structure, and the contour plots superimposed on the

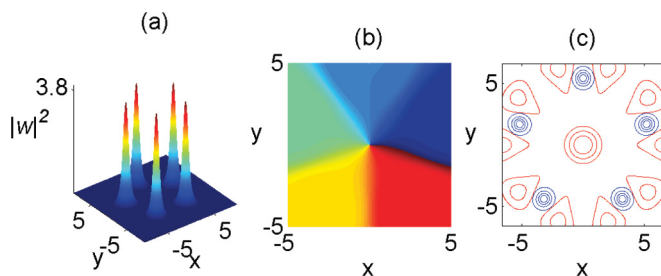


FIG. 3. (Color online) (a) Vortex profile centered at a lattice minimum away from the lattice center, with $r = 5.3918$; (b) the phase structure of the vortex; (c) the contour plot of the vortex humps superimposed on the underlying Penrose potential ($N = 5$).

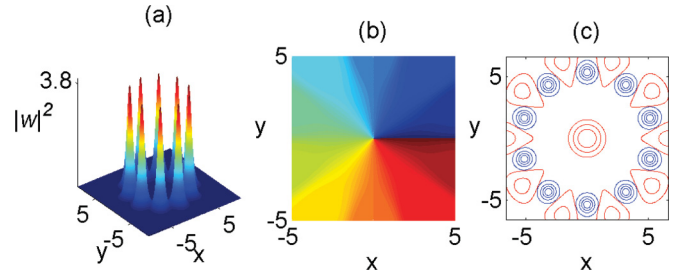


FIG. 4. (Color online) (a) Vortex profile centered at the lattice minima; (b) the phase structure of the vortex; (c) the contour plot of the vortex humps superimposed on the underlying Penrose potential ($N = 5$).

underlying Penrose potential at the lattice minimum are shown in Fig. 4.

B. Vortex solitons on lattice maxima

Vortex solitons on lattice maxima including both five- and ten-hump vortex solitons on a Penrose lattice are investigated. A five-hump vortex centered at the maximum of the potential in Fig. 5 is obtained when $\theta_n = 2\pi n/5$. Both the five-hump and the ten-hump vortices are found for the propagation constant $\mu = 0.8$ and $A = 1, r = 6.2504$.

The ten-hump vortex located at the lattice maximum is shown in Fig. 6; in this case $\theta_n = \pi n/5$.

C. Dipole soliton at lattice minima

A dipole or two-phase localized vortex is also found for the Penrose lattice. We found a dipole centered at the lattice minimum with propagation constant $\mu = -2, A = 3,$ and $r = 2.3918$. The dipole profile, its phase structure, and the contour plot of the dipole humps superimposed on the underlying Penrose lattice are shown in Fig. 7.

D. Dipole soliton at the lattice maxima

A dipole centered at a lattice maximum is also found numerically; here $\mu = 0.8, A = 3,$ and $r = 6.2504$. The dipole profile, its phase structure, and the contour plot of the dipole humps superimposed on the underlying Penrose lattice are shown in Fig. 8.

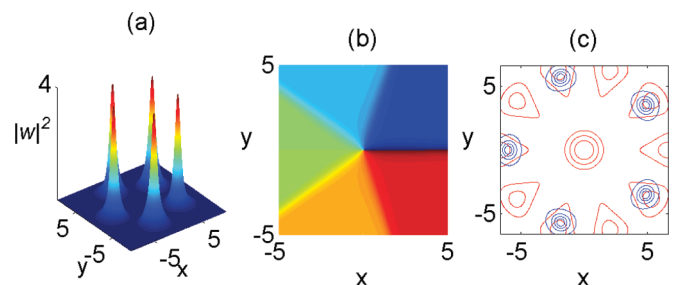


FIG. 5. (Color online) (a) Vortex profile centered at the lattice maximum with $r = 6.2504$; (b) the phase structure of the vortex; (c) the contour plot of the vortex humps superimposed on the underlying Penrose potential ($N = 5$).

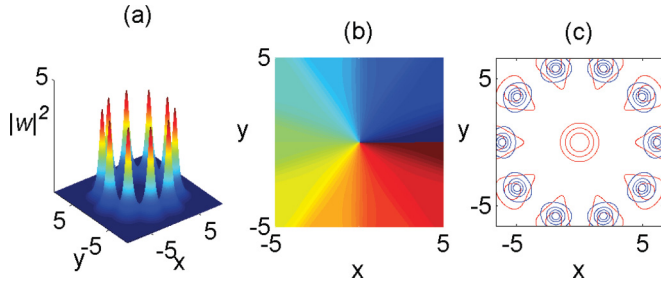


FIG. 6. (Color online) (a) Vortex profile centered at the lattice maximum with $r = 6.2504$; (b) the phase structure of the vortex; (c) the contour plot of the vortex humps superimposed on the underlying Penrose potential ($N = 5$).

IV. LINEAR INSTABILITY OF VORTEX AND DIPOLE SOLITONS

In this section the linearized evolution of vortex and dipole solitons is investigated. Let $u(x, y, z) = \exp(-i\mu z)[f(x, y) + \delta\tilde{u}(x, y, z)]$ be a perturbed mode, where $f(x, y)$ is the computed vortex or dipole soliton, and $\delta\tilde{u}$ is a small perturbation, where $|\delta| \ll 1$. Linearizing (1) gives

$$i \frac{\partial \tilde{u}}{\partial z} + \frac{\partial^2 \tilde{u}}{\partial x^2} + \frac{\partial^2 \tilde{u}}{\partial y^2} + [\mu - V(x, y) + 2|f|^2]\tilde{u} + f^2 \tilde{u}^* = 0. \quad (8)$$

We solve (8) with the Penrose potential over a sufficiently long distance. The initial condition $\tilde{u}(x, y, z = 0)$ is chosen as 1% random noise in amplitude and phase. Spatial finite differences for $\tilde{u}_{xx} + \tilde{u}_{yy}$ and a fourth-order Runge-Kutta method in z are employed. Figures 9–12 present the results of some of these simulations.

We first investigate five-humped vortex solitons. Figure 9 shows that the peak amplitudes of the vortex solitons increase rapidly with the propagation distance z . Similar unstable dynamics is observed for the cases of ten-humped vortices (see Figs. 10 and 11) as well as for a dipole (see Fig. 12).

We observe two recurring features in all these simulations:

(a) The blowup dynamics is a two-stage process: for a short distance (typically $z < 0.1$) the peak amplitude is nearly constant, followed by exponential growth. This makes sense, as the initial noise contains “all” stable and unstable components. Eventually, the most unstable component prevails.

(b) The instability growth rate is larger for solitons centered at lattice maxima. This suggests that, in general, the most

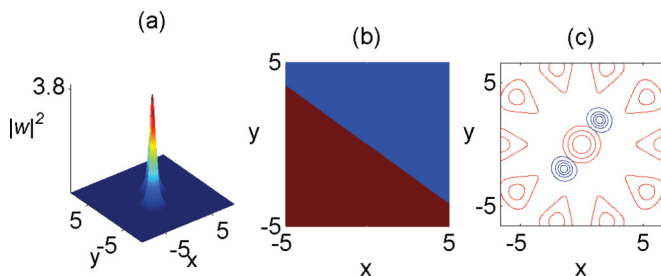


FIG. 7. (Color online) (a) A dipole profile centered at the lattice minimum of a Penrose potential with $r = 2.3918$; (b) the phase structure of the dipole; (c) the contour plot of the dipole humps superimposed on the underlying Penrose potential ($N = 5$).

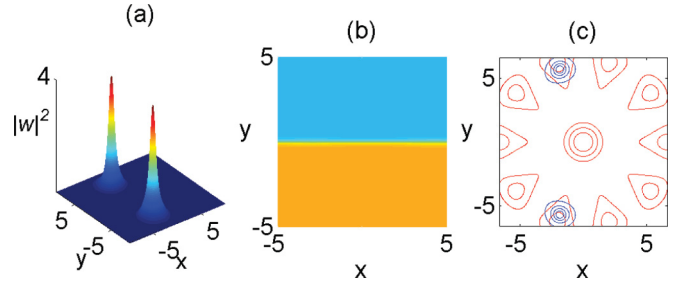


FIG. 8. (Color online) (a) A dipole profile centered at the lattice maximum with $r = 6.2504$; (b) the phase structure of dipole solitons; (c) the contour plot of dipole solitons superimposed on the underlying Penrose potential ($N = 5$).

unstable eigenvalue has a greater magnitude for solitons centered at lattice maxima compared with solitons centered at the (same) lattice minima (see also [15]).

V. NONLINEAR STABILITY OF VORTEX AND DIPOLE SOLITONS

Until now, we have studied the linear stability properties of vortex and dipole solitons that we found earlier. None of those vortex or dipole solitons are found to be linearly stable.

Another important issue is the nonlinear stability of these vortex and dipole solitons. The natural question to examine is whether linearly unstable vortex and dipole solitons are also nonlinearly unstable.

In order to examine the nonlinear stability of the vortex and dipole solitons found above, we directly compute Eq. (1), over a long distance ($z = 20$ or 30 is typically found to be sufficient) for both types of potential. As with the linearized problem, finite differences were used for the derivatives u_{xx} and u_{yy} and a fourth-order Runge-Kutta method to advance in z . The initial conditions were taken to be a vortex (or a dipole) with 1% random noise in amplitude and phase.

While examining the nonlinear stability, we evaluated the maximum amplitude versus the propagation distance, the change in the location of centers of mass and the phase structure of the vortex and dipole solitons. A stable soliton should nearly preserve (1) its peak amplitude, as opposed to undergoing self-focusing and /or finite-distance collapse; (2) its position on the lattice, i.e., it should be drift-stable (drift-unstable solitons are typically characterized by “humps” that drift from lattice maxima toward nearby minima); and (3)

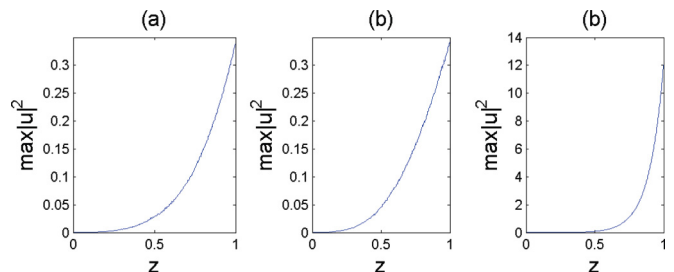


FIG. 9. (Color online) Linear evolution of the five-hump vortex on the Penrose lattice. Centered at (a) lattice minimum, close to the origin; (b) lattice minimum, away from the origin; (c) lattice maximum.

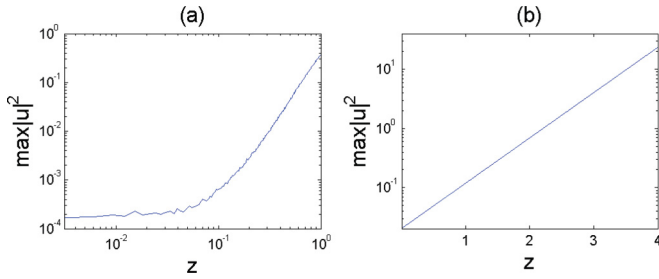


FIG. 10. (Color online) (a) Linear evolution of the ten-hump vortex on the Penrose lattice minimum on a double-logarithmic plot; (b) instability growth rate of (a).

its phase structure. If all three conditions are met then the soliton will be considered nonlinearly stable.

The center of mass is monitored as

$$(\langle x \rangle, \langle y \rangle) = \frac{1}{P} \iint_{-\infty}^{\infty} (x, y) |u|^2 dx dy. \quad (9)$$

Here, $P \equiv P[u] := \iint_{-\infty}^{\infty} |u|^2 dx dy$ is the soliton power.

The nonlinear stability of vortex and dipole solitons is investigated in the following sections separately.

A. Nonlinear stability of vortex solitons

Here we investigate the nonlinear stability of the vortex solitons that were obtained earlier. First, we examined the nonlinear stability properties of vortex solitons on lattice minima. We also investigated the effect of the location of the five-hump vortex. In this regard, we first considered the five-hump vortex (see Fig. 2) as the initial condition. The aforementioned five-hump vortex solitons are located close to the center of the lattice (the global maxima).

In Fig. 13, we show the maximum amplitude and the location of the center of mass versus the propagation distance z . It can be seen from this figure that the maximum amplitude of vortex solitons increases significantly just after approximately $z = 3$. This reveals that vortex solitons at lattice minima, located close to the center of the lattice, eventually become unstable and potentially collapse after a finite propagation distance z . The phase structure and contour plots are also shown in the same figure. An interesting phenomenon is observed during the nonlinear evolution; we see the amalgamation of two vortex humps near the propagation distance $z = 3.55$.

Similarly we note that the phase structure becomes entangled. In Fig. 14, the phase structures of the vortex on lattice

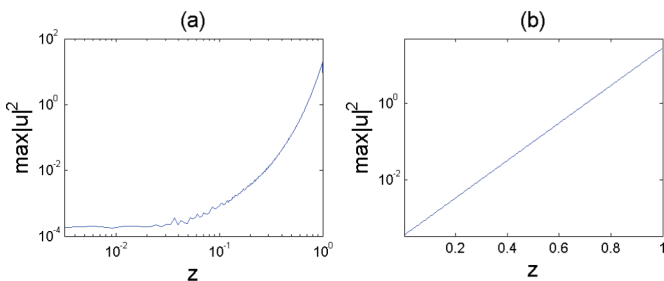


FIG. 11. (Color online) (a) Linear evolution of the ten-hump vortex on the Penrose lattice maximum on a double-logarithmic plot; (b) instability growth rate of (a).

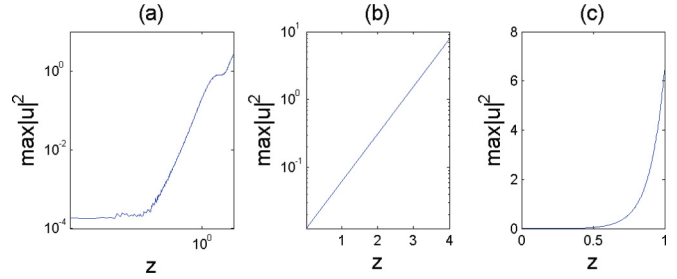


FIG. 12. (Color online) (a) Linear evolution of dipole solitons on a Penrose lattice minimum on a double-logarithmic plot; (b) instability growth rate of (a); (c) evolution on maxima.

minima located close to the lattice center are displayed for increasing propagation distances. As can be seen from the figure, the phase structure of the five-hump vortex starts to deteriorate at around $z = 1.5$. The phase structure of these vortex solitons is eventually disrupted and is not preserved after some propagation distance.

Next the nonlinear stability properties of the five-hump vortex on the lattice minima but farther away from the lattice center were examined in order to show the positive effect of increasing distance to the lattice center on nonlinear stability. To demonstrate this, as the initial condition, we took the five-hump vortex on a lattice minimum (farther away from the lattice center) shown in Fig. 3.

As can be seen from the Fig. 15, the maximum amplitude of these vortex solitons oscillates with relatively small amplitude and vortex humps stay nearly at the same place during the direct simulation (no drift instability). As a result of this fact, vortex solitons on the Penrose potential minimum, far away from the lattice center, are found to be nonlinearly stable. So one may conclude that, as the vortex humps get farther from

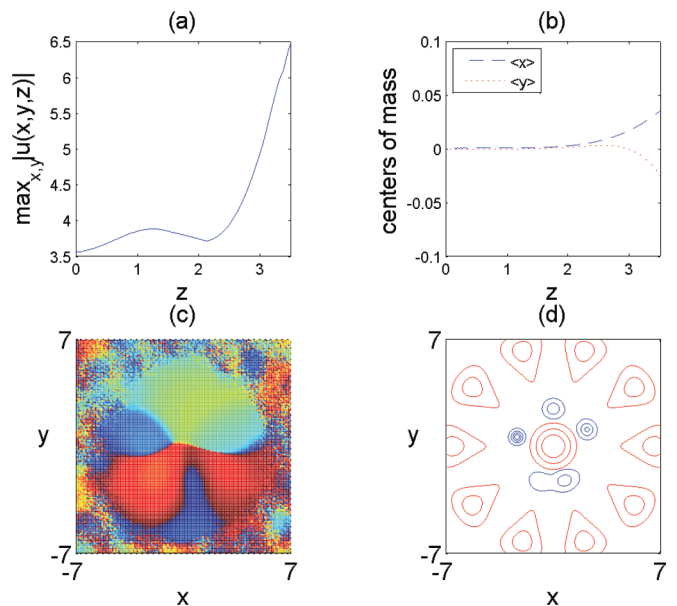


FIG. 13. (Color online) Amalgamation and collapse of five vortex solitons on a Penrose lattice. (a) Maximum amplitude as a function of propagation distance; (b) center of mass; (c) contour plot of the complex phase at $z = 3.55$; (d) contour plot of the amplitude at $z = 3.55$.

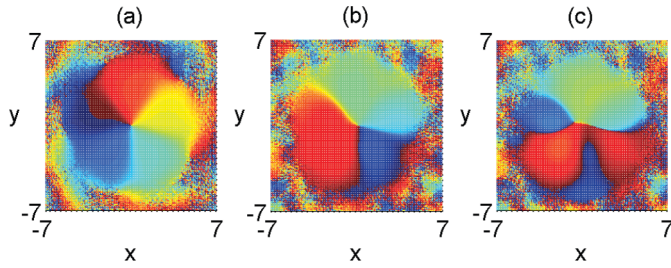


FIG. 14. (Color online) Phase structures of five vortex solitons on Penrose lattice minima, at various propagation distances: (a) $z = 1.5$; (b) $z = 3.5$; (c) $z = 3.55$ (just before the collapse).

each other, the nonlinear stability improves. The nonlinear stability holds despite the fact that we found this mode to be linearly unstable.

Next, the nonlinear stability properties of vortex solitons with ten humps at both lattice minima and maxima are also examined. In Fig. 16, we plot the maximum amplitude and the location of the centers of mass of a ten-hump vortex on Penrose lattice minima versus the propagation distance $z = 20$. The phase structure and the contour plots of the maximum amplitudes at the final point $z = 20$ are also depicted in the same figure.

It is seen that the maximum amplitude of these vortex solitons increases somewhat until $z = 8$ and after this value oscillates with relatively small amplitude. On the other hand, the phase structure breaks up after a few diffraction lengths ($z = 1$) (see Figs. 16 and 17).

The immediate breakup in the phase structure indicates the nonlinear instability of the ten-hump vortex solitons at Penrose lattice minima.

We investigated the nonlinear stability of the five- and ten-hump vortex solitons at the lattice maxima of the Penrose

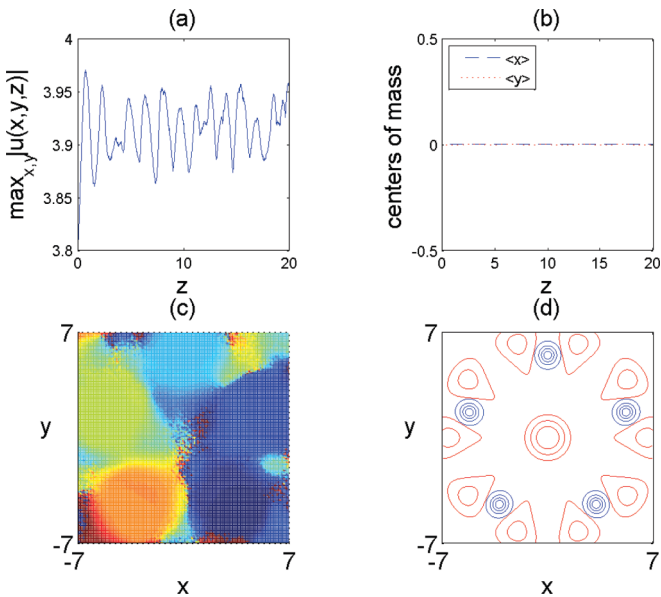


FIG. 15. (Color online) Nonlinear stability of five vortex solitons on a Penrose lattice. (a) Maximum amplitude as a function of propagation distance; (b) center of mass; (c) contour plot of the complex phase at $z = 20$; (d) contour plot of the amplitude at $z = 20$.

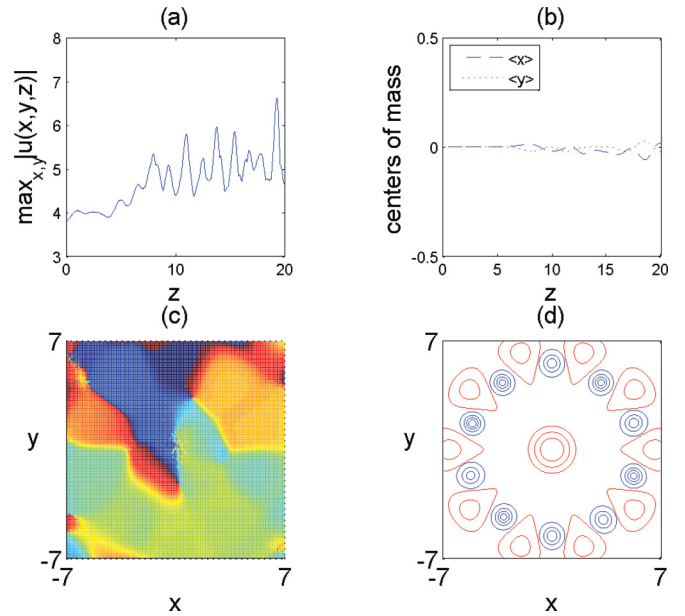


FIG. 16. (Color online) Nonlinear instability of ten vortex solitons on a Penrose lattice. (a) Maximum amplitude as a function of propagation distance; (b) center of mass; (c) contour plot of the complex phase at $z = 20$; (d) contour plot of the amplitude at $z = 20$.

potential by taking the five- (Fig. 5) and ten-hump (Fig. 6) vortices respectively on the Penrose lattice maxima as initial conditions. For both cases, we see that the maximum amplitudes increase quite sharply after a short propagation distance (around $z = 0.8$ and 0.75 for the five- and ten-hump cases, respectively), indicating nonlinear instability (see Figs. 18 and 19). The breakup in the phase is also observed in both figures. Further, during the evolution, both five-hump and ten-hump vortex solitons move from their initial locations (lattice maxima) to the lattice minima. Similar behavior was numerically observed in the case of fundamental lattice solitons by Ablowitz *et al.* [32] (see also [14–16]).

In view of the above investigations, only the five-humped vortex solitons on Penrose lattice minima (away from the origin) are found to be nonlinearly stable. The other lattice vortex solitons are found to be nonlinearly unstable due to either the sharp increment in the amplitude during the evolution, or breakup in the phase structure, or slipping of the centers of mass from lattice maxima through lattice minima (drift instability).

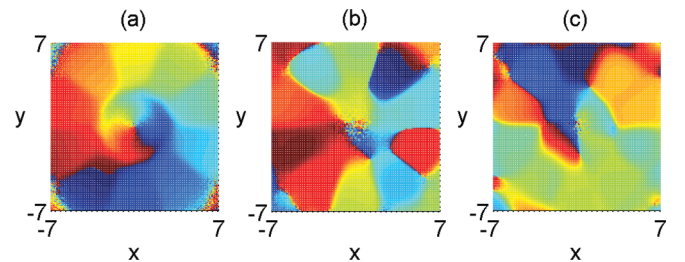


FIG. 17. (Color online) Phase structures of ten vortex solitons on a Penrose lattice, at various propagation distances: (a) $z = 1$; (b) $z = 10$; (c) $z = 20$.

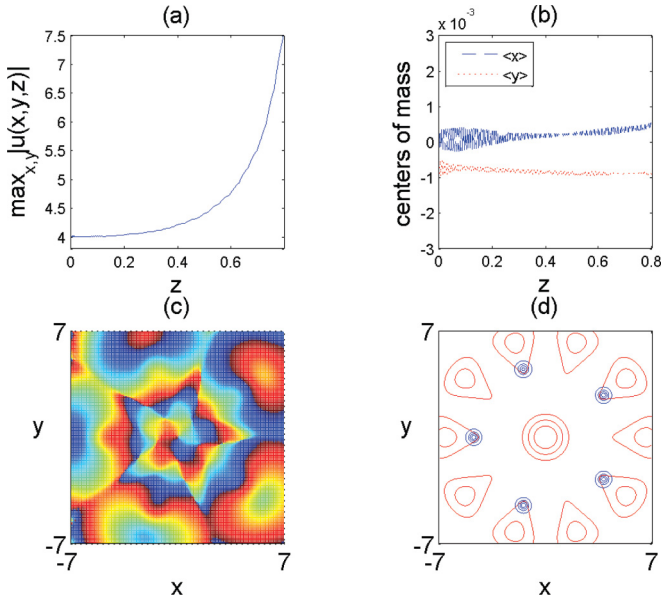


FIG. 18. (Color online) Collapse of five vortex solitons on a Penrose lattice. (a) Maximum amplitude as a function of propagation distance; (b) center of mass; (c) contour plot of the complex phase at $z = 0.8$; (d) contour plot of the amplitude at $z = 0.8$.

We also numerically obtained vortex solitons for a deep lattice, i.e., $V_0 = 300$. The nonlinear stability of five vortex solitons on a deep Penrose lattice is shown in Fig. 20. The propagation constant is taken to be $\mu = -2$ for this vortex.

For a relatively shallow potential ($V_0 = 10$), five vortex solitons centered on a Penrose lattice minimum (located close to the center of the lattice) have been found to be nonlinearly unstable due to the sharp increment in the maximum amplitude. Amalgamation of two vortex humps is also observed just

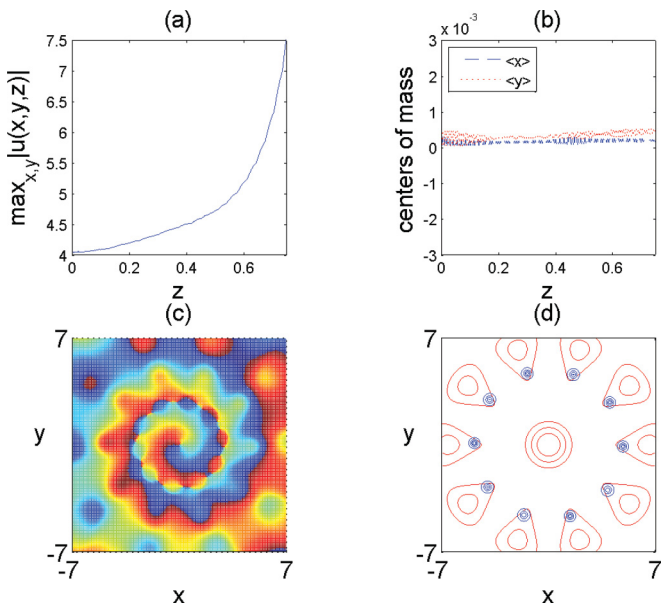


FIG. 19. (Color online) Collapse of ten vortex solitons at Penrose lattice maxima. (a) Maximum amplitude as a function of propagation distance; (b) center of mass; (c) contour plot of the complex phase at $z = 0.75$; (d) contour plot of the amplitude at $z = 0.75$.

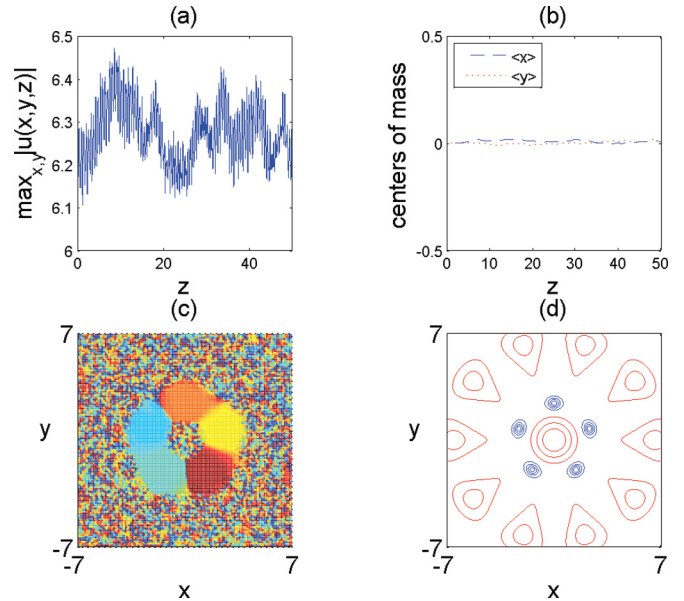


FIG. 20. (Color online) Nonlinear stability of the five-hump vortex on Penrose lattice minima for $V_0 = 300$, $z = 50$.

before the collapse occurs (see Fig. 13). On the other hand, when the lattice depth is increased to $V_0 = 300$, the maximum amplitude of the vortex solitons begins to oscillate with small amplitude, showing that the collapse is suppressed. It is also seen from Fig. 20(d) that there is no amalgamation. Therefore, the vortex solitons centered on a Penrose lattice minimum for the deep lattice case are found to be nonlinearly stable.

In Fig. 21, the nonlinear stability of a single vortex soliton centered at a lattice minimum is demonstrated. Figure 22 shows that the power for each of the humps of a vortex Penrose soliton (i.e., $P[u]/5$) decreases monotonically with the lattice depth when $V_0 \geq 0.5$ and scales approximately as $V_0^{-0.05}$ for large V_0 . The power of each hump is below the power of the homogeneous-medium fundamental soliton, i.e., the Townes mode, while it is slightly above the power of the fundamental soliton centered on Penrose lattice minima (close to the center). The “extra” power present in the vortex humps above the fundamental Penrose soliton is a consequence of the small overlap between adjacent humps.

B. Nonlinear stability of dipole solitons

In the last part of this work, we study the nonlinear stability properties of a dipole on a Penrose lattice. We first examine the nonlinear stability of dipole solitons on the Penrose lattice

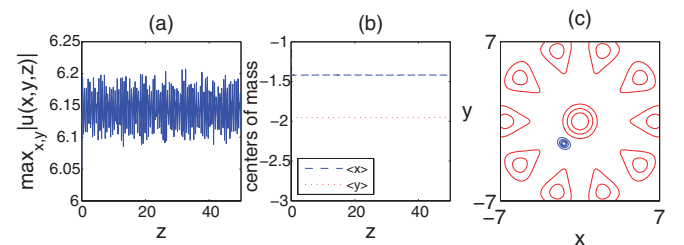


FIG. 21. (Color online) Nonlinear stability of a fundamental mode on Penrose lattice minima for $V_0 = 300$, $z = 50$.

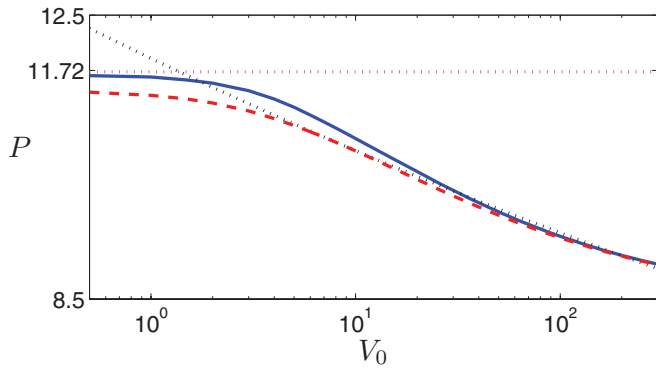


FIG. 22. (Color online) The power of each hump in a vortex Penrose soliton ($P[u]/5$, solid curve) vs the lattice depth. Also shown are the powers of the fundamental homogeneous-medium soliton (horizontal dots) and of the fundamental Penrose soliton centered at a local minimum near the origin ($11.9V_0^{-0.05}$, dashed curve below the solid curve), and the best power-law fit to the single-hump power (dash-dotted line).

minima that are previously shown in Fig. 7. These structures are found to be nonlinearly stable due to the conservation of the location and the phase structure and, at the same time, show only small oscillations in the maximum amplitude during the evolution (see Fig. 23). We recall, in contrast, that this dipole was shown to be linearly unstable.

The nonlinear stability properties of the dipole solitons on the Penrose lattice maxima are demonstrated in Fig. 24. The dipole solitons are found to be nonlinearly unstable since they exhibit strong localization after a few diffraction lengths and their phase structures break up. They also suffer from drift instability since the dipole humps both move from the lattice maxima toward nearby lattice minima immediately.

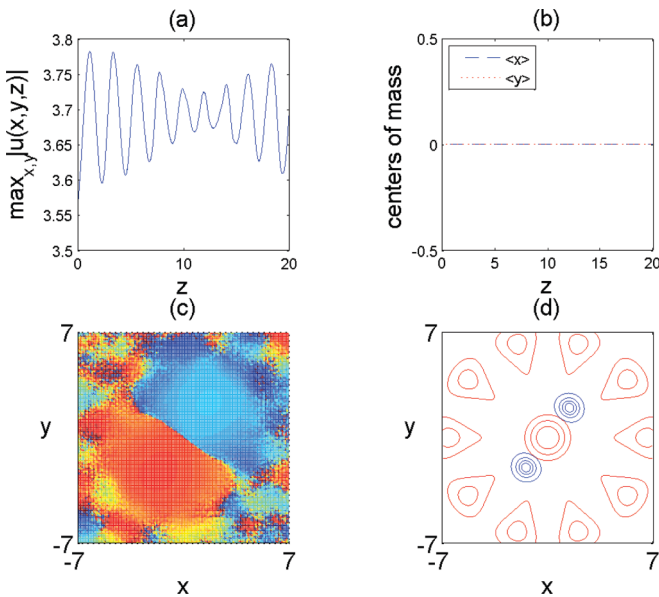


FIG. 23. (Color online) Nonlinear stability of a dipole on a Penrose lattice. (a) Maximum amplitude as a function of propagation distance; (b) center of mass; (c) contour plot of the complex phase at $z = 20$; (d) contour plot of the amplitude at $z = 20$.

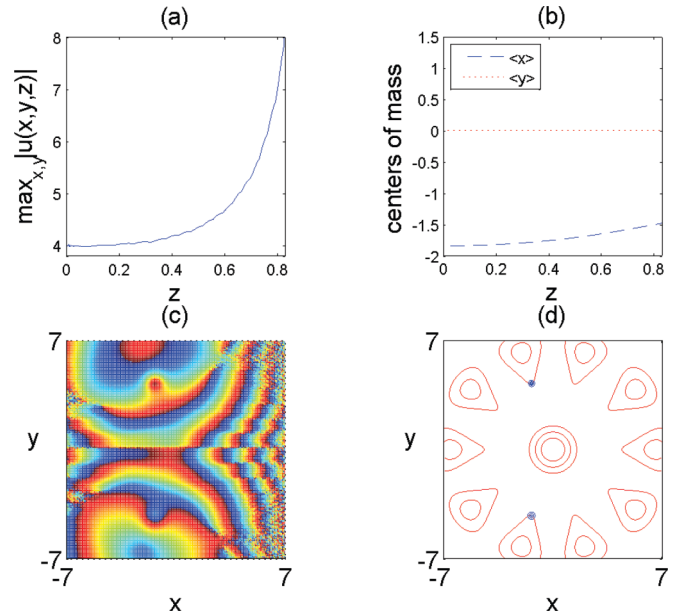


FIG. 24. (Color online) Collapse of dipoles on a Penrose lattice. (a) Maximum amplitude as a function of propagation distance; (b) center of mass; (c) contour plot of the complex phase at $z = 0.83$; (d) contour plot of the amplitude at $z = 0.83$.

Actually, this is expected since solitons on lattice maxima are typically drift-unstable [15] and also their power is above the collapse threshold (see [15,19]). However, comparing the collapse of the vortex and dipole solitons on Penrose lattices, we observe that the number of humps does not affect the collapse distance much. In fact, the collapse distances are more or less the same ($z \approx 0.3$) for five-hump and ten-hump vortex solitons, and for dipole solitons at Penrose lattice maxima ($z \approx 0.8, 0.75$, and 0.83 , respectively). Furthermore, the blowup dynamics are similar for all the above-mentioned vortex solitons. Therefore, these nonlinear stability properties may be predicted for triple vortex solitons centered at Penrose lattice maxima, should this be of interest.

VI. CONCLUSION

We have numerically investigated dipole and multiple vortex structures associated with Penrose lattices. The results of this study show that vortex and dipole solitons do exist on Penrose lattices and that they can be stable under suitable conditions. In particular, we show the numerical existence of vortex and dipole solitons, investigate their linear stability properties using direct simulations of the linearized NLS equation, and investigate their nonlinear stability properties using direct simulations of the NLS equation.

The simulations of the NLS equation showed the following: (i) Five-hump vortex solitons located far away from the lattice center are nonlinearly *stable*. (ii) The dipole and the vortex solitons situated at lattice maxima are nonlinearly *unstable*. In this case, the nonlinear instability occurs as a result of collapse, whereas the phase structure remains fairly stable until the collapse points. (iii) For vortex solitons centered at the Penrose lattice minimum (close to the origin), the amplitude (self-focusing) instability can be accompanied by degeneration

in the phase structure as a result of the amalgamation of two or more vortex humps. Vortex solitons for deep lattices were investigated as well, and it is found that the depth of the lattice can suppress instabilities. In addition, the simulations of the linearized NLS equation showed that vortex and dipole solitons can be nonlinearly stable, but linearly unstable. Consequently, linear stability cannot be considered as a necessary or sufficient condition for nonlinear stability for these types of lattice problems.

Although computational results do not prove rigorously the existence and stability of solutions, the results of this

study are encouraging for further investigations of localized nonlinear waves on quasicrystal and other complex lattices that can be created in Bose-Einstein condensates and nonlinear optics.

ACKNOWLEDGMENTS

M.J.A.'s research was partially supported by the US Air Force Office of Scientific Research under Grant No. FA9550-09-1-0250. N.A. was supported by Istanbul Technical University.

-
- [1] M. R. Matthews, B. P. Anderson, P. C. Haljan, D. S. Hall, C. E. Wieman, and E. A. Cornell, *Phys. Rev. Lett.* **83**, 2498 (1999).
- [2] J. R. Abo-Shaer, C. Raman, J. M. Vogels, and W. Ketterle, *Science* **292**, 476 (2001).
- [3] B. Luther-Davies and Y. S. Kivshar, *Phys. Rep.* **298**, 81 (1998).
- [4] O. Manela, O. Cohen, G. Bartal, J. W. Fleischer, and M. Segev, *Opt. Lett.* **29**, 2049 (2004).
- [5] J. W. Fleischer, G. Bartal, O. Cohen, O. Manela, M. Segev, J. Hudock, and D. N. Christodoulides, *Phys. Rev. Lett.* **92**, 123904 (2004).
- [6] B. Freedman, G. Bartal, M. Segev, R. Lifshitz, D. Christodoulides, and J. Fleischer, *Nature (London)* **440**, 1166 (2006).
- [7] H. Leblond, B. A. Malomed, and D. Mihalache, *Phys. Rev. A* **83**, 063825 (2011).
- [8] Y. V. Kartashov, B. A. Malomed, and L. Torner, *Rev. Mod. Phys.* **83**, 247 (2011).
- [9] M. I. Weinstein, *SIAM J. Math. Anal.* **16**, 472 (1985).
- [10] M. I. Weinstein, *Commun. Pure Appl. Math.* **39**, 51 (1986).
- [11] M. Weinstein, *Contemp. Math.* **99**, 213 (1989).
- [12] H. A. Rose and M. I. Weinstein, *Physica D* **30**, 207 (1988).
- [13] V. A. Brazhnyi, V. V. Konotop, and V. M. Pérez-Carcía, *Phys. Rev. Lett.* **96**, 060403 (2006).
- [14] Y. Sivan, G. Fibich, and M. I. Weinstein, *Phys. Rev. Lett.* **97**, 193902 (2006).
- [15] Y. Sivan, G. Fibich, B. Ilan, and M. I. Weinstein, *Phys. Rev. E* **78**, 046602 (2008).
- [16] B. Ilan, Y. Sivan, and G. Fibich, *Opt. Lett.* **36**, 397 (2011).
- [17] J. Yang and Z. H. Musslimani, *Opt. Lett.* **28**, 2094 (2003).
- [18] Z. H. Musslimani and J. Yang, *J. Opt. Soc. Am. B* **21**, 973 (2004).
- [19] M. J. Ablowitz, B. Ilan, E. Schonbrun, and R. Piestun, *Phys. Rev. E* **74**, 035601(R) (2006).
- [20] J. Yang, *New J. Phys.* **6**, 47 (2004).
- [21] H. Sakaguchi and B. A. Malomed, *Europhys. Lett.* **72**, 698 (2005).
- [22] J. Wang and J. Yang, *Phys. Rev. A* **77**, 033834 (2008).
- [23] H. Sakaguchi and B. A. Malomed, *Phys. Rev. E* **74**, 026601 (2006).
- [24] M. Senechal, *Quasicrystals and Geometry* (Cambridge University Press, Cambridge, 1995).
- [25] J. Yang, *Nonlinear Waves in Integrable and Nonintegrable Systems* (SIAM Society for Industrial and Applied Mathematics, Philadelphia, 2010).
- [26] V. I. Petviashvili, *Sov. J. Plasma Phys.* **2**, 257 (1976).
- [27] M. J. Ablowitz and Z. H. Musslimani, *Opt. Lett.* **30**, 2140 (2005).
- [28] T. I. Lakoba and J. Yang, *J. Comput. Phys.* **226**, 1668 (2007).
- [29] T. I. Lakoba and J. Yang, *J. Comput. Phys.* **226**, 1693 (2007).
- [30] T. I. Lakoba, *Physica D* **238**, 2308 (2009).
- [31] J. Yang, *J. Comput. Phys.* **228**, 7007 (2009).
- [32] M. J. Ablowitz, N. Antar, İ. Bakırtaş, and B. Ilan, *Phys. Rev. A* **81**, 033834 (2010).